

Design and Optimization of a Graphene-On-Silicon Nitride Integrated Waveguide Dual-Mode Electro-Absorption Modulator

Fernando Martín-Romero^{a,*}, Víctor J. Gómez^a

^aNanophotonics Technology Center, Universitat Politècnica de València, Valencia, 46022, Spain

ARTICLE INFO

Keywords:

Multimode modulator
Mode filter
Graphene
Silicon nitride
Hybrid integration

ABSTRACT

We present the design, simulation and optimization of a graphene-on-silicon nitride (GOSiN) integrated waveguide dual-mode electro-absorption modulator operating with a speed between 27–109 GHz and an energy consumption below 6 pJ/bit. This device individually modulates the TE_0 and TE_1 modes in a single-arm dual-mode waveguide with modulation depths up to 316 dB/cm and 273 dB/cm, respectively. It has promising applications in Multimode Division Multiplexing (MDM) systems, where single-mode modulation induces high losses and costs. We have started from the design of GOSiN TE_0 and TE_1 passive low-loss mode filters. Then, applying a gate voltage to graphene via transparent IHO electrodes, we have combined both filters and shown that the light absorption can be modulated to obtain four logical values in transmission: (0,0), (0,1), (1,0) and (1,1). Our proposed devices can potentially boost the development of efficient MDM systems for ultra-fast on-chip interconnections.

1. Introduction

Graphene integrated photonic devices have attracted a lot of attention in the last years [1]. Among all the unique properties of graphene, the tunability of its optical response via electrical gating and its ultra-high carrier mobility have allowed for interesting applications, such as optical isolators [2, 3], modulators [4–10] and photodetectors [11, 12]. Since it is a one-atom thick material, normal incidence of light in monolayer graphene will result in an absorption of only 2.3% of the incoming light. However, this can be overcome by hybrid integration of graphene in a silicon or silicon nitride waveguide, where the in-plane evanescent field of the confined modes strongly couples to graphene, increasing the absorption or phase change in the transmitted signal [13]. Such platforms are able to combine the advantageous properties of graphene with the well established technology of silicon photonics, which has resulted in proposals and demonstrations of several novel graphene-based integrated devices such as broadband high-speed photodetectors [11, 12], all-optical switches [4, 5] or ultra-fast single-mode electro-optical modulators [6, 7, 9, 10].

On the other hand, the sharp increase in global data traffic has resulted in new demanding requirements for transmission systems, which must be satisfied by novel photonic devices. These devices must have a larger bandwidth, a lower energy consumption and reduced fabrication costs [14]. In order to increase the transmission capacity inside a photonic chip, new multiplexing systems have been proposed. One that is currently under research is Mode Division Multiplexing (MDM) [15–17], which takes advantage of higher order waveguide modes to increase the single wavelength channel capacity of an on-chip transmission line. In a traditional

MDM system, the source signals emitted by the laser diode are modulated individually by single-mode electro-optical (EO) modulators [18]. Then, they are converted to higher order modes and multiplexed into a few-mode or dual-mode waveguide. This induces high costs, large device footprints and high insertion losses. However, replacing the single-mode modulators by a dual-mode or multi-mode modulator, would allow a more compact and efficient design, helping to overcome the cited disadvantages of MDM technology [19–21] (Fig. 1).

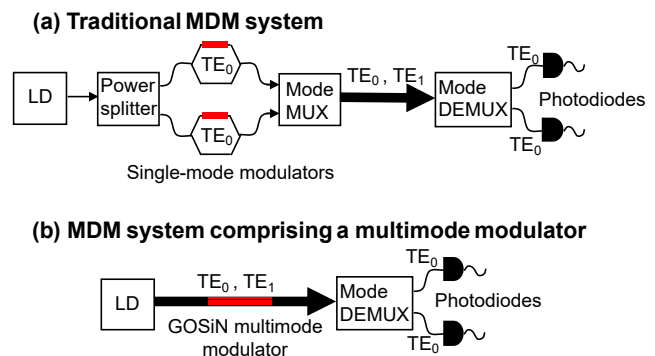


Figure 1: Mode Division Multiplexing system comprising (a) single-mode modulation, or (b) dual-mode modulation.

In this work, we present the design and simulation of an integrated graphene-on-silicon nitride (GOSiN) dual-mode electro-absorption modulator working at a wavelength of 1550 nm. To reduce modal crosstalk and spurious propagation in the modulator, we started by designing passive TE_0 and TE_1 mode filters [22, 23]. These mode filters consist of a SiN waveguide over which graphene nanoribbons are placed, acting as absorbers. Depending on the position and dimensions of the nanoribbons, one of the modes is absorbed and the other one is transmitted. For fixed dual-mode waveguide dimensions, we managed to minimize the length

*Corresponding author

✉ fmarrrom@ntc.upv.es (F. Martín-Romero); vjgomher@ntc.upv.es

(V.J. Gómez)

ORCID(s): 0009-0003-0930-3921 (F. Martín-Romero);

0000-0003-2364-8814 (V.J. Gómez)

and insertion losses of the filters by modifying the geometry of the graphene absorbers. Then, we designed a dual-mode modulator by combining both filters with transparent IHO (hydrogen-doped indium oxide) contacts, in order to actively tune the absorption of graphene. This allows the device to individually modulate the TE_0 and TE_1 signals. We have computed the modulation depth, the losses, the bandwidth and the energy consumption for both modes in the device. Given the ultra-high carrier mobility in graphene, the operation speed will be limited by the RC constant of the modulator, and not by the carrier transit time [24]. This can result in a modulation speed over 100 GHz, much higher than that achievable in a silicon dual-mode modulator [25].

2. Graphene-on-silicon nitride integrated waveguide mode filter

2.1. Concept and design of the mode filter

The design of the graphene-on-silicon nitride (GOSiN) integrated waveguide mode filter devices is shown in Fig. 2. It consists of a SiN core partially covered by graphene nanoribbons, and embedded in a SiO₂ cladding. We present two different filters: a TE_0 filter (Fig. 2a,b) and a TE_1 filter (Fig. 2c,d). In the first device, a graphene nanoribbon is covering a central stripe of the core, where the maximum intensity of the TE_0 mode is located. This will result in a strong absorption of the TE_0 mode, while the TE_1 mode is mainly transmitted. In the second device, two graphene nanoribbons are placed at the sides of the core, closer to each of the two intensity maxima of the TE_1 mode. This design is such that the TE_1 mode is strongly absorbed, and the TE_0 mode is transmitted.

A similar concept for a graphene-on-silicon (GOS) filter has been proposed in previous studies [22, 23]. However, the TE_1 mode presents a slower decay in the cladding for a silicon nitride waveguide (Fig. 2e), due to the lower index contrast in SiN. This allows to reduce mode overlapping, lowering the losses of the GOSiN mode filter, as the transmitted mode can be less affected by graphene absorption.

In order to assess the efficiency of the mode filters, we have computed the extinction ratio and selection ratio of these devices [22]. The extinction ratio is defined as the difference between the stop mode and the pass mode of the filter:

$$ER = \alpha_{stop} - \alpha_{pass}, \quad (1)$$

where α is the absorption coefficient in dB/cm units. For a given contrast, C (in dB units), between both modes, the length of the device can be computed as $L = C/ER$.

The selection ratio is defined as the ratio between the ER and the absorption coefficient of the pass-mode:

$$SR = ER/\alpha_{pass}. \quad (2)$$

For a given length of the device, the insertion losses, $IL = \alpha_{pass}L$ (in dB units), can be computed as $IL = C/SR$.

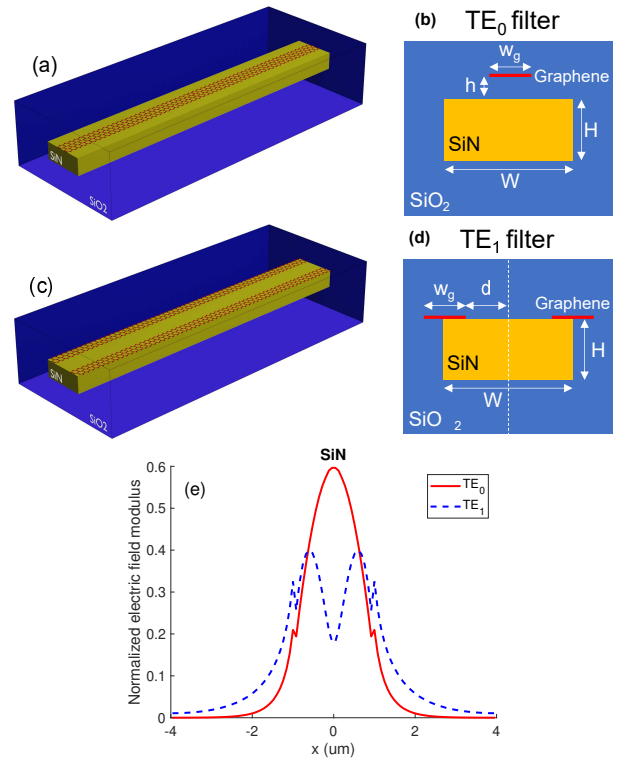


Figure 2: (a) Design and (b) geometrical parameters of the GOSiN TE_0 filter. (c) Design and (d) geometrical parameters of the GOSiN TE_1 filter. (e) Optical TE_0 and TE_1 modes in the silicon nitride waveguide.

In order to design a device with the minimum length and insertion losses, the product $L \times IL = C^2/ER \times SR$ should be minimized. Therefore, the figure of merit of the mode filter is equal to $ER \times SR$. The position and dimensions of graphene nanoribbons should be chosen in a manner that the product of the extinction ratio and the selection ratio is maximized.

2.2. Simulation methodology

Regarding the simulation of the graphene-on-silicon nitride mode filters, as well as the dual-mode modulators, we have explored two different approaches.

In the first approach, we have modelled graphene as a 2D material with a surface conductivity, σ_g , with a contribution corresponding to intraband absorption processes and another corresponding to interband absorption processes. Both contributions are given by the Kubo formula [26]:

$$\sigma_{intra} = \frac{2k_B T e^2}{\pi \hbar^2} \ln \left(2 \cosh \frac{E_f}{2k_B T} \right) \frac{i}{\omega + i\tau^{-1}}, \quad (3)$$

$$\sigma_{inter} = \frac{e^2}{4\hbar} \left(H(\omega/2) + i \frac{4\omega}{\pi} \int_0^\infty \frac{H(\Omega) - H(\omega/2)}{\omega^2 - 4\Omega^2} d\Omega \right), \quad (4)$$

$$\sigma_g = \sigma_{intra} + \sigma_{inter}, \quad (5)$$

where $H(\Omega) = \sinh(\frac{\hbar\Omega}{k_B T}) / [\cosh(\frac{\hbar\Omega}{k_B T}) + \cosh(\frac{E_F}{k_B T})]$, T is the temperature, E_f is the Fermi energy (electrochemical potential), $\omega = 2\pi f$ is the angular frequency of the signal, and τ is the charge relaxation time. In this model we consider $T = 300$ K and $\tau = 10^{-13}$ s.

Since single-layer graphene can be about 0.3 nm thick, its effect on the mode profile of the TE_0 and TE_1 modes can be neglected. We have computed the SiN waveguide modes by finite element method using COMSOL Multiphysics. The field distribution at the waveguide generates a certain surface current at the graphene nanoribbons, which will induce the absorption of light. The absorption coefficient, α , can be denoted by

$$\alpha = \frac{\text{Re}(\sigma_g)}{2P_{in}} \int_{w_g} |E_{\parallel}|^2, \quad (6)$$

where P_{in} is the total incident power at the waveguide cross-section and the square of the in-plane electric field magnitude is integrated over the width of the nanoribbon, w_g [13].

The second approach corresponds to the modelling of graphene as a bulk material with a thickness d . The permittivity of graphene is computed as follows [27]:

$$\epsilon = 1 + \frac{i\sigma_g}{\omega\epsilon_0 d}. \quad (7)$$

Following this approach, the modes for a graphene-covered SiN waveguide are computed. The absorption coefficient can be obtained from the imaginary part of the mode effective index, n_{eff} , as

$$\alpha = 40\pi(\log_{10}e)\text{Im}(n_{eff})/\lambda \quad (8)$$

This last method takes graphene into account during the mode analysis of the waveguide. However, it is also much more computationally expensive than the first method, and only shows a small offset in the results (as mentioned in Section 2.3). Taking this into account, the results discussed in the following sections correspond to the conductivity method.

2.3. Design optimization of the mode filter

The first step is to optimize the design of the GOSiN mode filter for a wavelength of 1550 nm. We have simulated the ER , SR and $ER \times SR$ parameters of the TE_0 and TE_1 modes for a dual-mode waveguide with fixed core dimensions, and variable graphene dimensions (Fig. 2b,d). We chose a low thickness of $H = 200$ nm for the core, so that the electric field is larger at the position of graphene. For such thickness, a width of $W = 1860$ nm ensures that the waveguide is dual-mode for TE polarization. In the case of the TE_0 filter, we optimized the width of the graphene nanoribbon, w_g , and the vertical separation between the nanoribbon and the top of the SiN core, h . Meanwhile, the

optimized parameters for the TE_1 filter were w_g and the horizontal separation between the center of the SiN core and each graphene nanoribbon, d .

The results obtained for each of the GOSiN filters are shown in Fig. 3, and they can be compared to those of simulated GOS filters with $W=1500$ nm and $H=200$ nm [22]. It is observed that the maximum figure of merit is higher in the case of GOSiN filters. The GOSiN TE_0 filter shows a maximum $ER \times SR$ value of 1350 dB/cm at $w_g = 500$ nm, while the corresponding simulation on GOS shows only 680 dB/cm at $w_g = 260$ nm. In both cases, the optimal design requires the graphene nanoribbons to be at $h = 0$, right on top of the core. Regarding the GOSiN TE_1 filter, a strong dependence on w_g is observed, unlike in GOS devices. For a horizontal separation of $d = 2$ μm with respect to the center of the core and a width of $w_g = 2$ μm , the $ER \times SR$ product is 833 dB/cm, which is already larger than the 330 dB/cm corresponding to the GOS TE_1 filter. Moreover, the figure of merit of the GOSiN TE_1 filter can be further improved by increasing the separation of the graphene nanoribbons from the core, while slightly reducing the extinction ratio of the device.

These optimization results can be used to determine the fabrication tolerance of the mode filters. For the TE_0 filter, if we define it as the interval of w_g values in which the figure of merit is above 90% of its maximum value, the tolerance of the GOSiN TE_0 filter is between 500-200 nm and 500+100 nm, while in GOS is of 250 ± 80 nm [22]. In the case of the TE_1 filter, the figure of merit can be further increased for higher values of d , and only drops down 90% of its maximum value for $d = 2000$ -200 nm. Meanwhile, the tolerance for d in GOS is 400 ± 50 nm.

It is worth mentioning that the bulk method has also been used for simulating the absorption coefficients and the figure of merit of the mode filters. However, the computational cost is much higher, and the results only show an increase of less than 10% in the absorption coefficients, with no changes on the behaviour of the device. Therefore, the conductivity method was the preferred approach through the remainder of this study.

3. Graphene-on-silicon nitride integrated waveguide electro-optic dual-mode modulator

3.1. Concept, design and optimization of the dual-mode modulator

After discussing the behaviour of the GOSiN mode filters, we present the concept and design of an electro-absorption GOSiN dual-mode modulator based on the same principle. The mode filter shows that it is possible to selectively absorb the TE_0 or the TE_1 mode. Taking into account that graphene absorption can be modulated by changing its Fermi energy level via gate voltage, then the absorption of each of these modes can be independently modulated. The aim of the dual-mode modulator is to generate ON-OFF logical values of the form (0,0), (0,1), (1,0) or (1,1), where

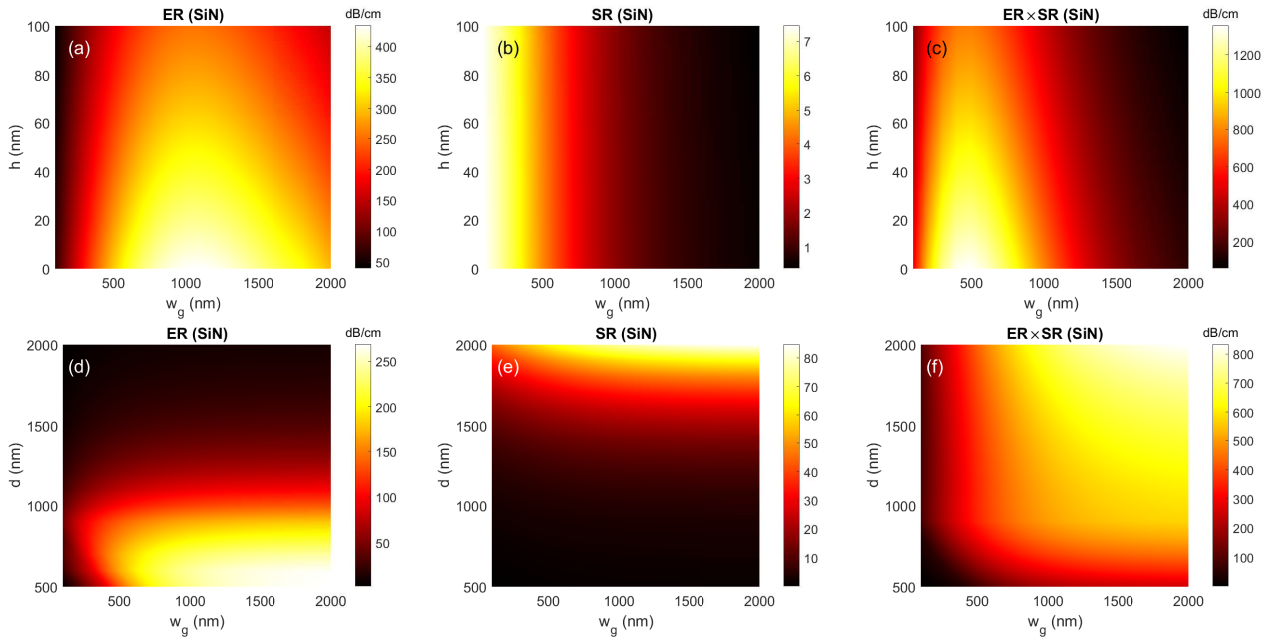


Figure 3: (a-c) ER, SR and ER×SR parameters in a GOSiN TE₀ filter as a function of the vertical position with respect to the top of the core (h) and the width (w_g) of the graphene nanoribbon. (d-f) ER, SR and ER×SR parameters in a GOSiN TE₁ filter as a function of the horizontal position with respect to the center of the core (d) and the width (w_g) of each graphene nanoribbon.

the first digit corresponds to the TE₀ signal, and the second one to the TE₁ signal.

The design of the device derives from the combination of both the TE₀ and the TE₁ filter. From the optical point of view, we have optimized the geometry of the device in order to achieve the four mentioned logical values. We have chosen the same fixed core dimensions as in Section 2.3 ($W=1860$ nm, $H=200$ nm) and varied the width of the graphene nanoribbons of the TE₀ and TE₁ filters (w_{g0} and w_{g1}), as well as the horizontal separation between the center of the SiN core and each of the TE₁ filter graphene nanoribbons (d). The design and geometry parameters are shown in Fig. 4.

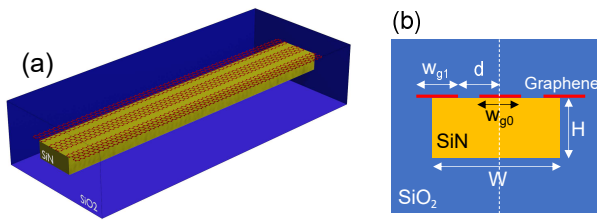


Figure 4: (a) Design and (b) dimensions involved in the GOSiN electro-optic dual-mode modulator.

In the simulations, the Fermi energy (or chemical potential) of graphene was varied between 0 and 1 eV independently on each of the filters, computing the absorption coefficient of each mode with the same method described for the mode filters. The results for three different designs are shown in Fig. 5. All three designs show a dependence of the absorption coefficient of the TE₀ mode mainly on the Fermi energy of the graphene corresponding to the TE₀

modulator. However, the first two designs show too much crosstalk between the TE₁ mode and the TE₀ modulator. Only the third case ($w_{g0}=200$ nm, $w_{g1}=1600$ nm, $d=1100$ nm) shows four differentiated regions corresponding to the four desired logical values. It can be observed how the absorption coefficient of the TE₀ mode depends mainly on the Fermi energy of the TE₀ modulator, while the same happens with the TE₁ mode and the TE₁ modulator.

In order to assess the efficiency of the dual-mode modulator, we have computed its modulation depth, which depends on the operation it is performing. There are two ON positions for the TE₀ mode, (1,0) and (1,1), as well as two OFF positions, (0,1) and (0,0). This results in four possible ON-OFF switching operations with different modulation depths. A similar discussion could be made for the TE₁ mode. Table 1 shows the maximum and minimum possible values of the modulation depth, as well as the maximum insertion losses, for each of the modes. As it can be observed, the MD of the TE₁ modulator is lower than the MD of the TE₀ modulator. Taking into account that the minimum MD of the TE₁ mode is the parameter which determines the minimum length of the device, the third design will result in a more compact device with less losses.

3.2. Dual layer GOSiN modulator

For the full design of the device, a dual-layer graphene modulator structure was considered, where instead of a single layer of graphene, each modulator comprises two layers of graphene separated by a spacer material, such as Al₂O₃. Each of the graphene layers act as contacts for the electro-optic modulation, forming a capacitor. The charge density, ρ , in the top and bottom layer is, respectively [9]:

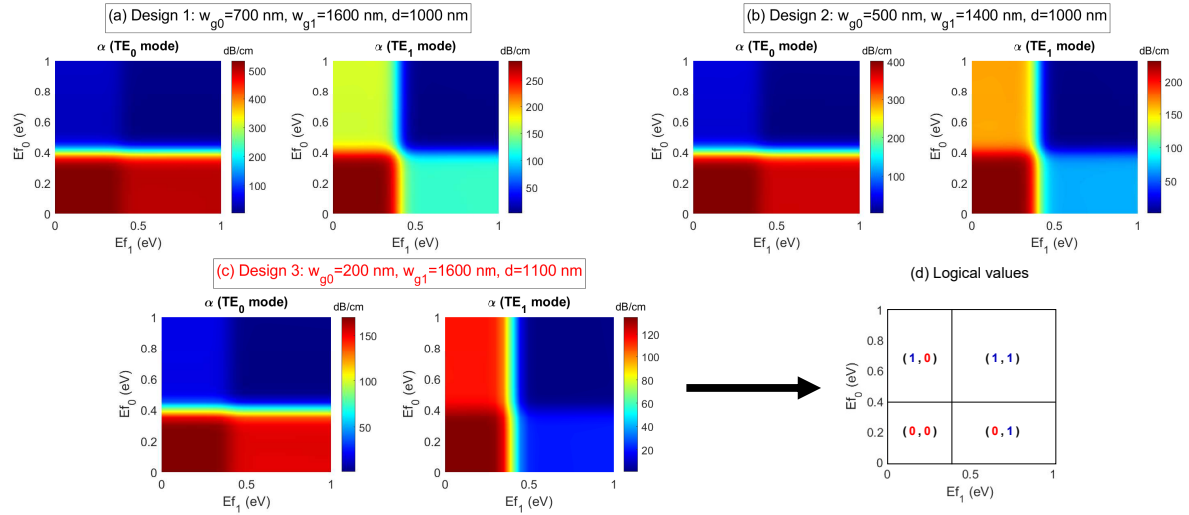


Figure 5: (a-c) Absorption coefficient of the TE₀ and TE₁ modulators for three different design parameters. (d) The third design shows a structure that can generate the four logical values: (0,0), (0,1), (1,0) and (1,1).

Table 1

Maximum and minimum modulation depth in three different GOSiN multimode modulator designs. Design 1: $w_{g0}=700$ nm, $w_{g1}=1800$ nm, $d=1000$ nm. Design 2: $w_{g0}=500$ nm, $w_{g1}=1400$ nm, $d=1000$ nm. Design 3: $w_{g0}=200$ nm, $w_{g1}=1600$ nm, $d=1100$ nm.

w_{g0} (nm)	w_{g1} (nm)	d (nm)	TE ₀			TE ₁		
			Max MD (dB/cm)	Min MD (dB/cm)	Max IL (dB/cm)	Max MD (dB/cm)	Min MD (dB/cm)	Max IL (dB/cm)
700	1600	1000	524	462	37	281	44	123
500	1400	1000	393	332	36	227	95	69
200	1600	1100	167	135	18	132	95	20

$$\rho_{top} = -en_b + \frac{1}{A} \int_{V_0}^{V_g} CdV \quad (9)$$

$$\rho_{bot} = -en_b - \frac{1}{A} \int_{V_0}^{V_g} CdV \quad (10)$$

where e is the electronic charge, n_b is the natural carrier density of graphene, A is the modulator surface, V_g is the gate voltage, V_0 is the bias voltage and C is the total capacitance. If the natural doping is approximately zero, then the top and bottom charge densities are $\rho_{top} = -\rho_{bot}$, and therefore the Fermi energy of both layers is $E_{f,top} = -E_{f,bot}$. Then, both layers act as gate contacts and signal modulators [6]. However, the natural doping can also be modified in order to achieve $\rho = 0$ in either the top or bottom layer. In such case, that layer acts only as a gate contact, while the other one modulates the signal [9]. Fig. 6 shows the simulation results for undoped graphene dual-layer modulators with different spacer thicknesses. It can be observed that adding a second layer of graphene improves the absorption of light, approximately duplicating the modulation depth per unit length of the modulators.

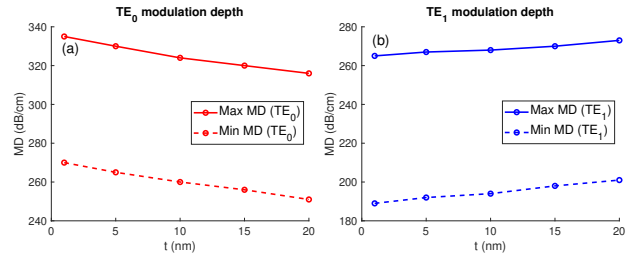


Figure 6: Maximum and minimum modulation depth of (a) TE₀ mode and (b) TE₁ mode for dual-layer GOSiN dual-mode modulator designs with different Al₂O₃ thicknesses, t .

3.3. Performance of the modulator

In practice, the full structure of the modulator presents some changes with respect to Fig. 4, so that the Fermi energy of graphene can be modified by applying a voltage. Fig. 7 shows a full design for the dual-mode integrated modulator where a graphene-Al₂O₃-graphene structure acts as a capacitor, similar to what can be found in the literature [19–21]. Instead of using metallic contacts, each capacitor is connected to hydrogen-doped indium oxide (IHO) electrodes. IHO is a transparent conductive oxide (TCO) that presents low absorption at $\lambda = 1550$ nm, so this choice of material contributes greatly to reduce the insertion losses of the

modulator [28, 29]. Nonetheless, given that the electrodes connected to the TE₀ modulator are closer to the waveguide core, they must be shorter than those connected to the TE₁ modulator in order to minimize losses. The device will not need two arms, since it is an electro-absorption modulator, which simplifies the design by avoiding a Mach-Zender interferometer structure. The dimensions and position of the graphene nanoribbons correspond to those of the design with $w_{g0}=200$ nm, $w_{g1}=1600$ nm and $d=1100$ nm.

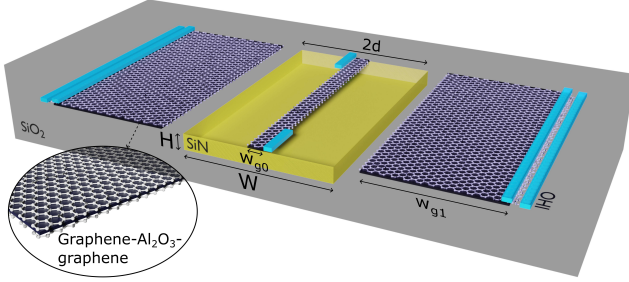


Figure 7: Schematic view of the proposed GOSiN electro-optic integrated waveguide dual-mode modulator including IHO electrodes.

In order to discuss the modulation speed of the device, the electronic bandwidth, $f_{3dB} = 1/(2\pi RC)$, must be computed for both the TE₀ and the TE₁ modulator. The bandwidth depends on the total resistance, R , and the total capacitance, C , of the device. Regarding the resistance, it depends on two contributions in series: the sheet resistance of the graphene nanoribbons, $R_g \approx 200\Omega/\square$ [6], and the sheet resistance of the IHO/graphene bilayer electrodes, $R_{el} \approx 237\Omega/\square$ [30]. It can be written as

$$R = 2R_g \frac{w_g}{l_g} + 2R_{el} \frac{w_{el}}{l_{el}}, \quad (11)$$

where w_g and l_g are the width and length of the graphene nanoribbon, as well as w_{el} and l_{el} are the width and length of the electrodes. A conservative estimate for a 50 nm thick IHO/graphene bilayer resistance can be obtained from the sheet resistance of a graphene/In₂O₃ bilayer of the same thickness [30]. Since IHO is hydrogen-doped indium oxide, the correlation in the chemical structure of both materials suggests a similar contact surface with graphene. The total capacitance, assuming undoped graphene, will be given by the plane-parallel graphene capacitor:

$$C = \epsilon_r \epsilon_0 w_g l_g / t, \quad (12)$$

where $\epsilon_r = 3$ is the relative permittivity of the spacer material (in this case, Al₂O₃ [21]), and t is the spacer thickness [1, 9, 31].

The voltage applied in order to modify the Fermi energy of graphene can be computed as follows [32]:

$$V_g - V_0 = \frac{E_f^2}{\hbar^2 v_f^2 \pi \eta}, \quad (13)$$

where $v_f=3 \times 10^6$ m/s is the Fermi velocity of graphene [32] and $\eta = \epsilon_0 \epsilon_r / te$ corresponds to a plane-capacitor model for the graphene modulator. The energy consumed per bit can be expressed as [33]:

$$E_{bit} = C(|V_g - V_0|^2 / 4) \quad (14)$$

We propose an example for the modulator geometry in which the length of the TE₀ and the TE₁ filters is 650 μ m and 750 μ m, respectively. The IHO electrodes would be 100 nm wide and 50 nm thick. In the case of the TE₁ modulator, they are 750 μ m long, while in the case of the TE₀ modulator, they are only 10 μ m long. For a spacer thickness of 20 nm, this leads to a modulation depth between 16 and 21 dB for the TE₀ mode and between 15 and 20 dB for the TE₁ mode. The insertion losses are between 0.2 and 2.6 dB for the TE₀ mode and between 0.2 and 2.8 dB for the TE₁ mode.

Fig. 8 shows the bandwidth and the energy consumption per bit as a function of the spacer thickness in the mentioned design, assuming a maximum achieved Fermi energy of around $E_f=0.6$ eV at the ON position. Increasing the thickness of the capacitors results in an improvement of the modulation speed, but also an increase in the energy consumed per bit. Therefore, there is a compromise between both parameters.

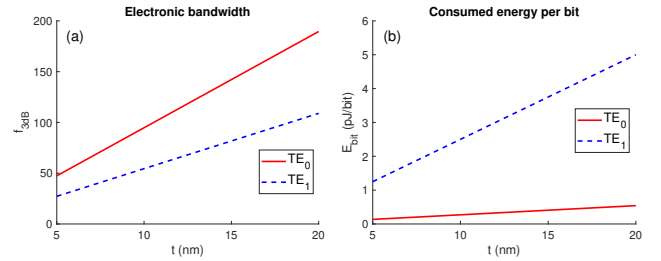


Figure 8: (a) Electronic 3dB bandwidth and (b) consumed energy per bit for the TE₀ and TE₁ modulators, as a function of the Al₂O₃ thickness, t .

The geometric parameters of the device may be modified in order to obtain a different performance. For instance, the length of the TE₁ electrodes can be made smaller in order to reduce the insertion losses. However, this increases the resistance of such contacts, thus decreasing the bandwidth of the device.

4. Discussion

Several dual-mode modulators have been theoretically proposed for implementation into a Mode Division Multiplexing system. Each design predicts different results in terms of modulation depth, insertion losses, modulation speed or energy consumption (Table 2). For instance, graphene-polymer waveguides show a low modulation depth per unit length (<60 dB/cm) and a higher energy consumption (>10 pJ/bit) [21]. In contrast, silicon dual-mode ring resonators, which have been experimentally demonstrated, are very compact. However, they can reach a more limited

Table 2

Comparison of the performance of our simulated device with respect to the state of the art.

*Estimate from provided results.

**Data not provided.

	Modes	Geometry	Footprint	Modulation depth (dB)	Insertion losses (dB)	Bandwidth (GHz)	E_{bit} (pJ/bit)
Our design (GOSiN electro-absorption modulator simulation)	2	Waveguide (one arm)	$5.4 \mu\text{m} \times 750 \mu\text{m}$	up to 16-21 (TE_0) up to 15-20 (TE_1)	0.2-2.6 dB (TE_0) 0.2-2.8 dB (TE_1)	~ 47 -190 (TE_0) ~ 27 -109 (TE_1)	0.14-0.54 (TE_0) 1.25-5.00 (TE_1)
Graphene-polymer waveguide modulator (simulation) [21]	3	Waveguide (one arm)	$\sim 16 \mu\text{m}^* \times 1 \text{ cm}$	23	~ 3.9 (TE_0)* ~ 4.4 (TE_{01})* ~ 4.5 (TE_{10})*	31.5 (TE_0) 2.8 (TE_{01}) 4 (TE_{10})	12.6 (TE_0) 94.5 (TE_{01}) 126 (TE_{10})
GOSiN phase modulator (simulation) [20]	2	MZI (two arms)	$\sim 0.5 \text{ mm}^2*$	19.3 (TE_0) 21.7 (TE_1)	1.7-2.4 (TE_0) 0.6-1.1 (TE_1)	1	16
GOS phase modulator (simulation) [35]	2	MZI (two arms)	0.5 mm^2	27.3 (TE_0) 31.4 (TE_1)	1.6-6.5 (TE_0) 2.3-7.2 (TE_1)	**	1.365
Silicon ring modulator (experiment) [25, 34]	2	Racetrack resonator, two mode converters	$\sim 26.3 \mu\text{m}^* \times >29 \mu\text{m}^*$	4.17 (TE_0) 2.7 (TE_1)	~ 1.5 (TE_0)* ~ 3.5 (TE_1)*	5	2*
GOS ring modulator (simulation) [19]	2	Racetrack resonator	$\sim 90 \mu\text{m}^* \times \sim 348.5 \mu\text{m}^*$	14.7 (TE_0) 9.2-15.3 (TE_1)	0.03-0.06	**	**

modulation speed of a few GHz [25, 34]. Graphene-silicon dual-mode micro-racetrack resonators represent an interesting approach due to their compact design, however their efficiency in terms of speed and energy consumption is yet to be studied [19].

The use of graphene nanoribbons over a silicon nitride waveguide allows the independent modulation of the TE modes in a dual-mode waveguide. By electrically tuning the conductivity of graphene, one may modify the absorption of light in the waveguide or its phase change. Phase modulation increases the dimensions of the device, since it requires a Mach-Zender interferometer structure with two arms. To the best of our knowledge, the proposed electro-refractive modulation designs show modulation depths of 275 dB/cm (TE_0) and 310 dB/cm (TE_1) [20]; or also 341 dB/cm (TE_0) and 760 dB/cm (TE_1) [35], with the disadvantages of having a lower modulation speed (1 GHz or less), higher losses (up to ~ 7 dB for the TE_0 or the TE_1 mode at a GOS modulator) and requiring each of the two modulators to be set in a different waveguide, resulting in a larger footprint (0.5 mm^2). This problem can be overcome by opting for direct absorption modulation, thus avoiding the need for two

waveguides and resulting in a simpler and more compact design.

Our GOSiN electro-absorption dual-mode modulator presents a more compact structure with a single waveguide combining a TE_0 and a TE_1 modulator that show modulation depths up to 251-316 dB/cm and 201-273 dB/cm, respectively. The use of IHO instead of metallic electrodes reduces the insertion losses while allowing to place the contacts closer to the capacitors, increasing the modulation speed of the device. Using the design of Fig. 7 with nanoribbons that are $650 \mu\text{m}$ and $750 \mu\text{m}$ long, respectively, the ultra-high carrier mobility in graphene allows modulation speeds between 27 and 109 GHz. The energy consumption can go approximately between 1.39 pJ/bit and 5.54 pJ/bit. There is a compromise between the bandwidth/speed of the device and its energy consumption. While the increase in the energy consumption with the capacitor thickness is slow, specially for the TE_0 modulator, the slope of the bandwidth increase is much steeper. Therefore, keeping the thickness inside a range between 5 and 20 nm allows to design an ultra-fast device while staying under the 10 pJ/bit marked by the state of the art in multi-mode modulators.

5. Conclusion

We have proposed an ultra-fast integrated dual-mode modulation photonic device that can be incorporated to a silicon photonic integrated circuit. This device allows to independently and simultaneously modulate two different waveguide modes, by a direct electrical tuning of the absorption of graphene. The incorporation of such dual-mode modulator to an on-chip MDM transmission line would allow to reduce energy consumption and increase the speed of data traffic.

The GOSiN mode filters present an improvement with respect to state of the art GOS simulations, greatly reducing the losses of the transmitted mode. Regarding the dual-mode modulator, it shows large modulation depths limited by the TE_1 modulator (251-316 dB/cm for TE_0 mode and 201-273 dB/cm for TE_1 mode), and generally improves the state of the art in graphene multi-mode modulators. The device is capable of ultra-fast modulation, reaching speeds up to around 190 GHz for the TE_0 modulator and 109 GHz for the TE_1 modulator. It shows an energy consumption between 0.14 and 0.54 pJ/bit for TE_0 modulation and between 1.25 pJ/bit and 5.00 pJ/bit for TE_1 modulation. It also presents a more reduced footprint with respect to other graphene multi-mode modulators.

In summary, the proposed device paves the way to an integrated MDM system for efficient ultra-fast on-chip interconnections.

Acknowledgement

F.M.R. acknowledges financial support from the Generalitat Valenciana (Project: CIACIF/2022/188). V.J.G. acknowledges financial support from the Generalitat Valenciana (CDEIGENT/2020/009) and to the AGENCIA ESTATAL DE INVESTIGACIÓN of Ministerio de Ciencia e Innovación (CNS2023-145093). All authors acknowledge financial support from AGENCIA ESTATAL DE INVESTIGACIÓN of Ministerio de Ciencia e Innovación (PID2020-118855RB-I00) and to the European Regional Development Fund (ERDF) (IDIFEDER/2020/041, IDIFEDER/2021/061). This study formed part of the Advanced Materials program and was supported by Ministerio de Ciencia e Innovación (MCIN) with funding from European Union NextGenerationEU (PRTR-C17.I1) and by Generalitat Valenciana (MFA/2022/025). This study also formed part of the Quantum Communications program and was supported by Ministerio de Ciencia e Innovación (MCIN) with funding from European Union NextGenerationEU (PRTR-C17.I1) and by Generalitat Valenciana (COMCUANTICA/003).

References

[1] F. Bonaccorso, Z. Sun, T. Hasan, A. C. Ferrari, Graphene photonics and optoelectronics, *Nature Photonics* 4 (9) (2010) 611–622, number: 9 Publisher: Nature Publishing Group. doi:10.1038/nphoton.2010.186. URL <https://www.nature.com/articles/nphoton.2010.186>

[2] J. Ma, X. Xi, Z. Yu, X. Sun, Hybrid graphene/silicon integrated optical isolators with photonic spin-orbit interaction, *Applied Physics Letters* 108 (15) (2016) 151103, publisher: American Institute of Physics. doi:10.1063/1.4945715. URL <https://aip.scitation.org/doi/10.1063/1.4945715>

[3] M. Zarei, F. Nazari, M. K. Moravvej-Farshi, Tunable optical isolator using Graphene-photonic crystal-based hybrid system, *Physica Scripta* 96 (9) (2021) 095502, publisher: IOP Publishing. doi:10.1088/1402-4896/ac03df. URL <https://dx.doi.org/10.1088/1402-4896/ac03df>

[4] M. Ono, M. Hata, M. Tsunekawa, K. Nozaki, H. Sumikura, H. Chiba, M. Notomi, Ultrafast and energy-efficient all-optical switching with graphene-loaded deep-subwavelength plasmonic waveguides, *Nature Photonics* 14 (1) (2020) 37–43, number: 1 Publisher: Nature Publishing Group. doi:10.1038/s41566-019-0547-7. URL <https://www.nature.com/articles/s41566-019-0547-7>

[5] G. X. Ni, L. Wang, M. D. Goldflam, M. Wagner, Z. Fei, A. S. McLeod, M. K. Liu, F. Keilmann, B. Özyilmaz, A. H. Castro Neto, J. Hone, M. M. Fogler, D. N. Basov, Ultrafast optical switching of infrared plasmon polaritons in high-mobility graphene, *Nature Photonics* 10 (4) (2016) 244–247, number: 4 Publisher: Nature Publishing Group. doi:10.1038/nphoton.2016.45. URL <https://www.nature.com/articles/nphoton.2016.45>

[6] M. Liu, X. Yin, X. Zhang, Double-Layer Graphene Optical Modulator, *Nano Letters* 12 (3) (2012) 1482–1485, publisher: American Chemical Society. doi:10.1021/nl204202k. URL <https://doi.org/10.1021/nl204202k>

[7] Y. Hu, M. Pantouvaki, J. Van Campenhout, S. Brems, I. Asselberghs, C. Huyghebaert, P. Absil, D. Van Thourhout, Broadband 10 Gb/s operation of graphene electro-absorption modulator on silicon, *Laser & Photonics Reviews* 10 (2) (2016) 307–316, eprint: <https://onlinelibrary.wiley.com/doi/pdf/10.1002/lpor.201500250>. doi:10.1002/lpor.201500250. URL <https://onlinelibrary.wiley.com/doi/abs/10.1002/lpor.201500250>

[8] J.-S. Shin, J. T. Kim, Broadband silicon optical modulator using a graphene-integrated hybrid plasmonic waveguide, *Nanotechnology* 26 (36) (2015) 365201, publisher: IOP Publishing. doi:10.1088/0957-4484/26/36/365201. URL <https://dx.doi.org/10.1088/0957-4484/26/36/365201>

[9] S. J. Koester, M. Li, High-speed waveguide-coupled graphene-on-graphene optical modulators, *Applied Physics Letters* 100 (17) (2012) 171107, publisher: American Institute of Physics. doi:10.1063/1.4704663. URL <https://aip.scitation.org/doi/10.1063/1.4704663>

[10] E. Heidari, H. Dalir, F. M. Koushyar, B. M. Nouri, C. Patil, M. Miscuglio, D. Akinwande, V. J. Sorger, Integrated ultra-high-performance graphene optical modulator, *Nanophotonics* 11 (17) (2022) 4011–4016, publisher: De Gruyter. doi:10.1515/nanoph-2021-0797. URL <https://www.degruyter.com/document/doi/10.1515/nanoph-2021-0797/html>

[11] P. Ma, Y. Salamin, B. Baeuerle, A. Josten, W. Heni, A. Emboras, J. Leuthold, Plasmonically Enhanced Graphene Photodetector Featuring 100 Gbit/s Data Reception, High Responsivity, and Compact Size, *ACS Photonics* 6 (1) (2019) 154–161, publisher: American Chemical Society. doi:10.1021/acsp Photonics.8b01234. URL <https://doi.org/10.1021/acsp Photonics.8b01234>

[12] Y. Gao, L. Tao, H. K. Tsang, C. Shu, Graphene-on-silicon nitride waveguide photodetector with interdigital contacts, *Applied Physics Letters* 112 (21) (2018) 211107, publisher: American Institute of Physics. doi:10.1063/1.5026303. URL <https://aip.scitation.org/doi/10.1063/1.5026303>

[13] S. J. Koester, M. Li, Waveguide-Coupled Graphene Optoelectronics, *IEEE Journal of Selected Topics in Quantum Electronics* 20 (1) (2014) 84–94, conference Name: IEEE Journal of Selected Topics in Quantum Electronics. doi:10.1109/JSTQE.2013.2272316.

[14] K. S. Novoselov, V. I. Fal'ko, L. Colombo, P. R. Gellert, M. G. Schwab, K. Kim, A roadmap for graphene, *Nature* 490 (7419) (2012) 192–200, number: 7419 Publisher: Nature Publishing Group.

- doi:10.1038/nature11458.
URL <https://www.nature.com/articles/nature11458>
- [15] B. Stern, X. Zhu, C. P. Chen, L. D. Tzuan, J. Cardenas, K. Bergman, M. Lipson, On-chip mode-division multiplexing switch, *Optica* 2 (6) (2015) 530–535, publisher: Optica Publishing Group. doi:10.1364/OPTICA.2.000530.
URL <https://opg.optica.org/optica/abstract.cfm?uri=optica-2-6-530>
- [16] H. Jia, T. Zhou, L. Zhang, J. Ding, X. Fu, L. Yang, Optical switch compatible with wavelength division multiplexing and mode division multiplexing for photonic networks-on-chip, *Optics Express* 25 (17) (2017) 20698–20707, publisher: Optica Publishing Group. doi:10.1364/OE.25.020698.
URL <https://opg.optica.org/oe/abstract.cfm?uri=oe-25-17-20698>
- [17] Y. Liu, K. Xu, S. Wang, W. Shen, H. Xie, Y. Wang, S. Xiao, Y. Yao, J. Du, Z. He, Q. Song, Arbitrarily routed mode-division multiplexed photonic circuits for dense integration, *Nature Communications* 10 (1) (2019) 3263, number: 1 Publisher: Nature Publishing Group. doi:10.1038/s41467-019-11196-8.
URL <https://www.nature.com/articles/s41467-019-11196-8>
- [18] D. Dai, J. Wang, Y. Shi, Silicon mode (de)multiplexer enabling high capacity photonic networks-on-chip with a single-wavelength-carrier light, *Optics Letters* 38 (9) (2013) 1422–1424, publisher: Optica Publishing Group. doi:10.1364/OL.38.001422.
URL <https://opg.optica.org/ol/abstract.cfm?uri=ol-38-9-1422>
- [19] G. Yue, Z. Xing, H. Hu, Z. Cheng, G.-W. Lu, T. Liu, Graphene-based dual-mode modulators, *Optics Express* 28 (12) (2020) 18456–18471, publisher: Optica Publishing Group. doi:10.1364/OE.394409.
URL <https://opg.optica.org/oe/abstract.cfm?uri=oe-28-12-18456>
- [20] J. Wang, X. Zhang, Y. Chen, Y. Geng, Y. Du, X. Li, Design of a graphene-based silicon nitride multimode waveguide-integrated electro-optic modulator, *Optics Communications* 481 (2021) 126531. doi:10.1016/j.optcom.2020.126531.
URL <https://www.sciencedirect.com/science/article/pii/S0030401820309494>
- [21] T. Lian, M. Zhu, S. Sun, X. Sun, Y. Che, B. Lin, X. Wang, D. Zhang, Mode-selective modulator and switch based on graphene-polymer hybrid waveguides, *Optics Express* 30 (13) (2022) 23746–23755, publisher: Optica Publishing Group. doi:10.1364/OE.460966.
URL <https://opg.optica.org/oe/abstract.cfm?uri=oe-30-13-23746>
- [22] P. Xing, K. J. A. Ooi, D. T. H. Tan, Ultra-broadband and compact graphene-on-silicon integrated waveguide mode filters, *Scientific Reports* 8 (1) (2018) 9874, number: 1 Publisher: Nature Publishing Group. doi:10.1038/s41598-018-28076-8.
URL <https://www.nature.com/articles/s41598-018-28076-8>
- [23] Z. Xing, C. Li, Y. Han, H. Hu, Z. Cheng, J. Wang, T. Liu, Waveguide-integrated graphene spatial mode filters for on-chip mode-division multiplexing, *Optics Express* 27 (14) (2019) 19188–19195, publisher: Optica Publishing Group. doi:10.1364/OE.27.019188.
URL <https://opg.optica.org/oe/abstract.cfm?uri=oe-27-14-19188>
- [24] J. Goscinia, D. T. H. Tan, Theoretical investigation of graphene-based photonic modulators, *Scientific Reports* 3 (1) (2013) 1897, publisher: Nature Publishing Group. doi:10.1038/srep01897.
URL <https://www.nature.com/articles/srep01897>
- [25] J. Liu, J. Du, W. Shen, L. Zhou, W. Zhang, Z. He, Silicon multi-mode micro-ring modulator for improved robustness to optical nonlinearity, *Optics Letters* 48 (14) (2023) 3729–3732, publisher: Optica Publishing Group. doi:10.1364/OL.496944.
URL <https://opg.optica.org/ol/abstract.cfm?uri=ol-48-14-3729>
- [26] A. Andryieuski, A. V. Lavrinenko, Graphene metamaterials based tunable terahertz absorber: effective surface conductivity approach, *Optics Express* 21 (7) (2013) 9144–9155, publisher: Optica Publishing Group. doi:10.1364/OE.21.009144.
URL <https://opg.optica.org/oe/abstract.cfm?uri=oe-21-7-9144>
- [27] V. Sorianello, M. Midrio, M. Romagnoli, Design optimization of single and double layer Graphene phase modulators in SOI, *Optics Express* 23 (5) (2015) 6478–6490, publisher: Optica Publishing Group. doi:10.1364/OE.23.006478.
URL <https://opg.optica.org/oe/abstract.cfm?uri=oe-23-5-6478>
- [28] E. Yang, B. Hu, Fabrication of High Transmittance and High Mobility Transparent Conductive Oxide Films: Hydrogen-doped Indium Oxide, *Journal of Physics: Conference Series* 2510 (1) (2023) 012011. doi:10.1088/1742-6596/2510/1/012011.
URL <https://iopscience.iop.org/article/10.1088/1742-6596/2510/1/012011>
- [29] J. J. Seoane, J. Parra, J. Navarro-Arenas, P. Sanchis, Enhanced BaTiO₃/Si₃N₄ integrated photonic platform with VO₂ technology for large-scale neuromorphic computing [Invited], *Optical Materials Express* 13 (11) (2023) 3266–3276, publisher: Optica Publishing Group. doi:10.1364/OME.501920.
URL <https://opg.optica.org/ome/abstract.cfm?uri=ome-13-11-3266>
- [30] S. Lee, M. Kim, S.-Y. Cho, D.-J. Lee, H.-M. Kim, K.-B. Kim, Electrical properties of graphene/In₂O₃ bilayer with remarkable uniformity as transparent conducting electrode, *Nanotechnology* 31 (9) (2020) 095708. doi:10.1088/1361-6528/ab599c.
URL <https://iopscience.iop.org/article/10.1088/1361-6528/ab599c>
- [31] L. Ji, Y. Gao, Y. Xu, X. Sun, C. Wu, Y. Wu, D. Zhang, High Figure of Merit Electro-Optic Modulator Based on Graphene on Silicon Dual-Slot Waveguide, *IEEE Journal of Quantum Electronics* 54 (6) (2018) 1–7, conference Name: IEEE Journal of Quantum Electronics. doi:10.1109/JQE.2018.2870579.
- [32] H. Shu, Z. Su, L. Huang, Z. Wu, X. Wang, Z. Zhang, Z. Zhou, Significantly High Modulation Efficiency of Compact Graphene Modulator Based on Silicon Waveguide, *Scientific Reports* 8 (1) (2018) 991, number: 1 Publisher: Nature Publishing Group. doi:10.1038/s41598-018-19171-x.
URL <https://www.nature.com/articles/s41598-018-19171-x>
- [33] M. R. Watts, W. A. Zortman, D. C. Trotter, R. W. Young, A. L. Lentine, Vertical junction silicon microdisk modulators and switches, *Optics Express* 19 (22) (2011) 21989–22003, publisher: Optica Publishing Group. doi:10.1364/OE.19.021989.
URL <https://opg.optica.org/oe/abstract.cfm?uri=oe-19-22-21989>
- [34] J. Liu, J. Du, W. Shen, G. Zhou, L. Zhou, W. Zhang, K. Xu, Z. He, Ultrahigh extinction ratio silicon micro-ring modulator by MDM resonance for high speed PAM-4 and PAM-8 signaling, *Optics Express* 30 (14) (2022) 25672–25684, publisher: Optica Publishing Group. doi:10.1364/OE.461594.
URL <https://opg.optica.org/oe/abstract.cfm?uri=oe-30-14-25672>
- [35] J. Wang, H. Qiu, Z. Wei, Y. Chen, Y. Geng, Y. Du, Z. Cheng, X. Li, Design of a Graphene-Based Waveguide-Integrated Multimode Phase Modulator, *IEEE Photonics Journal* 13 (4) (2021) 1–6, conference Name: IEEE Photonics Journal. doi:10.1109/JPHOT.2021.3089602.